PLOS ONE

RESEARCH ARTICLE

Probabilistic Optically-Selective Single-molecule Imaging Based Localization Encoded (POSSIBLE) microscopy for ultra-superresolution imaging

Partha Pratim Mondal *

Nanobioimaging Lab, Department of Instrumentation & Applied Physics, Indian Institute of Science, Bangalore, INDIA

* partha@iap.iisc.ernet.in

Citation: Pratim Mondal P (2020) Probabilistic Optically-Selective Single-molecule Imaging Based Localization Encoded (POSSIBLE) microscopy for ultra-superresolution imaging. PLoS ONE 15(11): e0242452. https://doi.org/10.1371/journal.pone.0242452

Editor: Ireneusz Grulkowski, Nicolaus Copernicus University, POLAND

Received: July 28, 2020

Accepted: November 3, 2020

Published: November 16, 2020

Data Availability Statement: All relevant data are within the manuscript and its Supporting information files.

Funding: The author(s) received no specific funding for this work.

Competing interests: The authors have declared that no competing interests exist.

Abstract

To be able to resolve molecular-clusters it is crucial to access vital information (such as, molecule density, cluster-size, and others) that are key in understanding disease progression and the underlying mechanism. Traditional single-molecule localization microscopy (SMLM) techniques use molecules of variable sizes (as determined by its localization precision (LP)) to reconstruct a super-resolution map. This results in an image with overlapping and superimposing PSFs (due to a wide size-spectrum of single-molecules) that undermine image resolution. Ideally, it should be possible to identify the brightest molecules (also termed as the **fortunate molecules**) to reconstruct ultra-superresolution map, provided sufficient statistics is available from the recorded data. Probabilistic Optically-Selective Single-molecule Imaging Based Localization Encoded (POSSIBLE) microscopy explores this possibility by introducing a narrow probability size-distribution of single-molecules (narrow size-spectrum about a predefined mean-size). The reconstruction begins by presetting the mean and variance of the narrow distribution function (Gaussian function). Subsequently, the dataset is processed and single-molecules are filtered by the Gaussian function to remove unfortunate molecules. The fortunate molecules thus retained are then mapped to reconstruct an ultra-superresolution map. In-principle, the POSSIBLE microscopy technique is capable of infinite resolution (resolution of the order of actual single-molecule size) provided enough fortunate molecules are experimentally detected. In short, bright molecules (with large emissivity) holds the key. Here, we demonstrate the POSSIBLE microscopy technique and reconstruct single-molecule images with an average PSF sizes of $\sigma \pm \Delta\sigma = 15 \pm 10$ *nm*, 30 ± 2 *nm* & 50 ± 2 *nm*. Results show better-resolved Dendra2-HA clusters with large cluster-density in transfected NIH3T3 fibroblast cells as compared to the traditional SMLM techniques. Cluster analysis indicates densely-packed HA molecules, HA-HA interaction, and a surge in the number of HA molecules per cluster post 24 Hrs of transfection. The study using POSSIBLE microscopy introduces new insights in influenza biology. We anticipate exciting applications in the multidisciplinary field of disease biology, oncology, and biomedical imaging.

I. Introduction

Imaging molecular processes with true molecular-resolution is the ultimate goal of light microscopy. This is largely eluded due to the diffraction of light which sets a lower bound on the resolution-limit [1, 2]. However, recent microscopy techniques such as, STED [3], fPALM [4], STORM [5], PALM [6], SIM [7] GSDIM [8] SOFI [9], PAINT [10, 11], SMILE [12, 13], MINFLUX [14] and others techniques [15–23] have surpassed this limit [1, 2]. The above techniques are far-from achieving truly molecular-scale resolution and thus are incapable of functional imaging with ultra-high-resolution (preferably in the range of single molecule length-scales). Hence it becomes imperative to develop technique that can explore sub-10 nm domain.

Single molecule localization microscopy rely on the fact that each detected molecules can be localized within a certain distance about its centroid. This determines its size and point spread function (PSF). The localization precision (LP) of a molecule is heavily dependent on the number of photons emitted by the molecule. So, a low photon number count for a recorded molecule is most likely to produce large PSF leading to a poorly-resolved image and vice-versa. A better way to resolve single molecules would be to selectively choose the fortunate molecules that emits large number of photons, thereby reducing localization uncertainty and its size. Existing SMLM techniques (fPALM/PALM) have large variability in their sizes (or LPs) since the PSFs have large size-spectrum ranging from few tens to few hundred nanometers. So, these super-resolution techniques are most likely to produce images with large mean resolution. On the other hand, a image reconstructed using fortunate molecules (having small PSFs and narrow size distribution) would lead to better resolution. Such a map is useful since existing localization microscopy confront situations where the molecules exhibit mixed emission properties (accounting for both weak and strong emissions) and incorporation of these molecules to build-up a map results in compromised resolution. Hence, a better strategy would be to look for fortunate molecules during data acquisition and record enough molecules to reconstruct the image. In a multi-resolution setup, one can define multiple Gaussians to classify molecules into strong, moderate and weak emitters based on their photon count. This helps to built a multi-resolution map of jumbled clusters which otherwise were poorly resolved by the existing SMLM techniques.

Here, we propose a new localization technique (termed as, POSSIBLE microscopy) which is capable of producing multi-resolution single molecules maps. In principle, the technique allow actual-molecular resolution (in the range of few-nanometers) provided the detection of bright photoactivable probes is achieved. To investigate viral infection due to influenza, we studied Hemagglutinin (HA) expressed in NIH3T3 fibroblast cells [24], its distribution and number density. These parameters are critical for viral replication and subsequent release of bud particles from infected cells [25]. Although existing super-resolution microscopy techniques show the presence of clusters during infection [26, 27], it has never allowed in-depth study of molecular clusters due to limited resolution. This requires immediate attention since intra-cluster resolution and packing-fraction are essential to determine the rate of infection. Our results reveal the existence of dense molecular sub-clusters (within large clusters) and enhanced #molecules /cluster post 24 Hrs of infection in HA transfected NIH3T3 cells. These informations are vital for developing antiviral drugs for disrupting HA assembly in order to subside the infection.

In this article, we propose a technique that can extend the resolution obtained by traditional localization microscopy. The proposed method explores for fortunate molecules that can be better localized (small average size and narrow variance) using a probability distribution of molecule-size (or equivalently LP). This technique can be used to explore resolution of the order of actual molecule dimension (sub-10 *nm* resolution) for live biological specimens.

II. Results

POSSIBLE microscopy has the ability to discern details within molecular systems such as macro-molecular clusters. In this study, we employ POSSIBLE microscopy to analyze HA clusters during influenza infection and compare it with the existing SMLM techniques.

A. POSSIBLE multiresolution microscopy

POSSIBLE microscopy looks for fortunate molecules that falls in the chosen Gaussian distribution with predefined LP mean and variance. In general, localization microscopy techniques utilize all the recorded single molecule PSFs with a well-defined localization precision that determines their size. So, the reconstructed map is a collection of single molecules / PSFs with localization precision varying from few tens to hundred nanometers. This results in blurred clusters due to overlapping PSFs (corresponding to single molecules) of varying sizes. To overcome the resolution obstructed by large PSFs, it may be possible to construct maps with fortunate molecules (that have relatively small PSFs).

In this article, we report a new multi-resolution optical microscopy technique to resolve molecular clusters (see, Fig 1). A possible yet effective way to address this would be to extract fortunate molecules from a large dataset of recorded single molecules. All the molecules have to pass through the probabilistic Gaussian filter test and depending upon their respective probability, they are selected to the set that represent the reconstructed image with desired resolution (calculated based on PSF size and size-variance).

Fig 2 show images obtained using multiple Gaussian filters. The single molecule events as recorded by the detector is shown in Fig 2A. Three different Gaussian distribution were considered based on their size (or equivalently their LP): poorly-resolved ($G(\sigma_{lp}, \Delta\sigma_{lp}) = G(50nm, 2nm)$), moderately-resolved ($G(30nm, 2nm)$) and highly-resolved ($G(15nm, 10nm)$) as shown in Fig 2B. A cartoon representing σ vs $\Delta\sigma$ along with their LP means is also shown. The recorded raw dataset depicting single molecule blinking can be seen in S1 Video, and the corresponding dataset displaying the extracted fortunate molecules using Gaussian filters are shown in S2 Video. The fortunate molecules are extremely bright (so, they are better localized), and are marked by white boxes (see, S2 Video). The reconstructed images along with the LP bar-plot are shown in Fig 2C. The (σ, $\Delta\sigma$) were chosen such that we get nearly equal number of

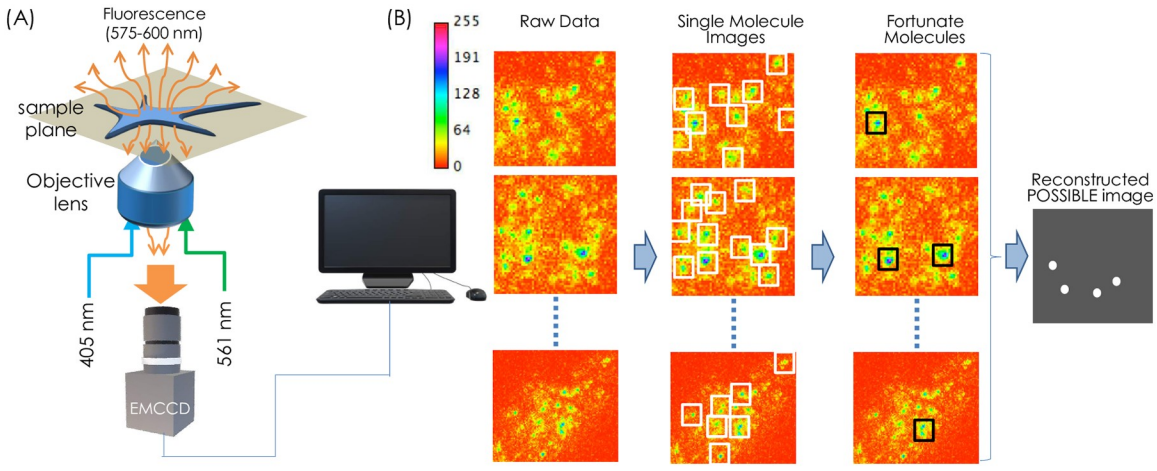

Fig 1. POSSIBLE microscopy, (A) The schematic diagram of optical setup, (B) Computational processes for determining the single molecules from the raw data after background subtraction and thresholding. This is followed by Gaussian filtering to retain the fortunate molecules for reconstructing POSSIBLE image.

https://doi.org/10.1371/journal.pone.0242452.g001

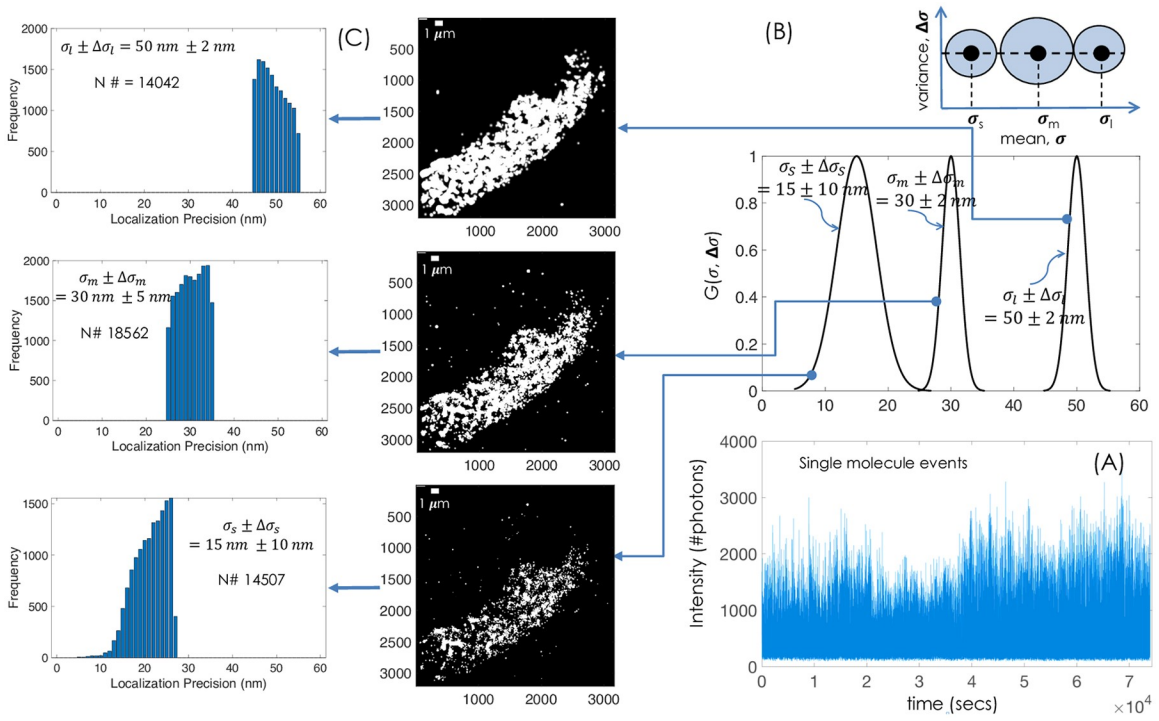

Fig 2. Multiresolution ultra-superresolution imaging using POSSIBLE microscopy. (A) The histogram of single molecule images as recorded by the EMCCD detector (Andor 897 iXon Ultra). (B) Three different Gaussian filters ($G(\sigma_s, \Delta\sigma_s)$, $G(\sigma_m, \Delta\sigma_m)$ and $G(\sigma_l, \Delta\sigma_l)$) for reconstructing 3 distinct POSSIBLE images. Schematic of $(\sigma, \Delta\sigma)$ space is also shown, (C) Reconstructed images with the corresponding localization precision histogram for highly-resolved molecules (corresponding to $G(\sigma_s, \Delta\sigma_s)$), moderately-resolved molecules ($G(\sigma_m, \Delta\sigma_m)$) and poorly-resolved molecules ($G(\sigma_l, \Delta\sigma_l)$), respectively. Scale bar is 1 μm.

https://doi.org/10.1371/journal.pone.0242452.g002

molecules in each distribution to enable comparison. The corresponding histograms for localization precision are also displayed. They represent the frequency of occurrence of single molecule with specific $(\sigma, \Delta\sigma)$. The number of molecules $(N\#)$ for $G(\sigma_l, \Delta\sigma_l)$, $G(\sigma_m, \Delta\sigma_m)$ and $G(\sigma_s, \Delta\sigma_s)$ are 14042, 18562 and 14507, respectively. Obviously, this shows that the recorded raw data has relatively large number of moderately-resolved molecules. In fact, several experiments show small statistics for highly-resolved molecules indicating significantly lower occurrence of molecules that emit large number of photons. Visually, the reconstructed super-resolution map reveals that the clusters are better-resolved for $G(\sigma_s, \Delta\sigma_s) = G(15nm, 10nm)$ as compared to $G(50nm, 2nm)$ and $G(30nm, 2nm)$. This is due to the fact that map generated by $G(\sigma_s, \Delta\sigma_s)$ has smaller PSFs compared to those for $G(\sigma_m, \Delta\sigma_m)$ and $G(\sigma_l, \Delta\sigma_l)$. So, the reconstruction of super-resolution image with fortunate molecules (falling in the distribution, $G(15nm, 10nm)$) result in ultra-high resolution.

B. Comparison with SMLM microscopy

To demonstrate the advantages of POSSIBLE microscopy, a comparison with the state-of-the-art SMLM (fPALM/PALM) was carried out. To ascertain fare comparison, we have ensured that same number of molecules were used to represent reconstructed image. Fig 3A shows the transmission image of the HA transfected NIH3T3 fibroblast cell and the region being imaged (white dotted square). Fig 3B shows POSSIBLE reconstructed image built from highly-resolved single molecules (i.e., $G(15\ nm, 10\ nm)$). A total of 14507 molecules out of 173448 recorded molecules (from 10,000 frames) have passed the Gaussian filtering process and found qualified

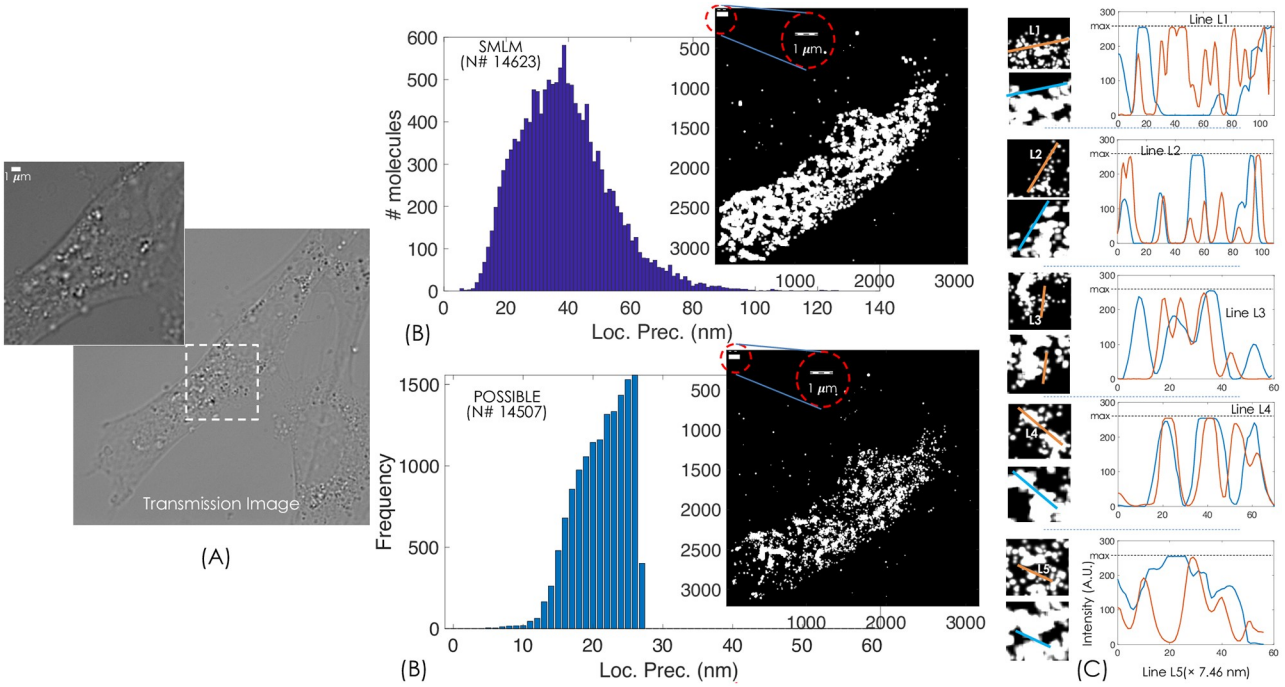

Fig 3. Comparison of POSSIBLE microscopy with SMLM (PALM/fPALM). (A) The transmission image of the cell. (B) Both SMLM and POSSIBLE reconstructed images are shown along with the histogram for number of molecules / frequency vs. LP. (C) Intensity plots along the lines, $L1 - L5$ for five different clusters. The comparison is carried out with almost equal number of molecules ($\#N$) to represent molecular clusters in the cell. Scale bar is 1 μm.

https://doi.org/10.1371/journal.pone.0242452.g003

to represent the reconstructed image. The second part of Fig 3B shows super-resolution image obtained using traditional SMLM microscopy (with actual molecule size or LP). The image is reconstructed using 14623 single molecules. To gain better insight in the reconstructed super-resolution maps, few clustered regions were chosen and the intensity along selected lines $L1 - L5$ were plotted as shown in Fig 3C. Here red and blue lines indicate POSSIBLE and traditional SMLM respectively. Visual inspection and intensity plots show better-resolved structures for POSSIBLE microscopy. Specifically, the intensity plots are able to bring out the details of molecule rearrangement within a small cluster. This is due to the fact that single molecules used to reconstruct POSSIBLE microscopy has a mean size of $\approx$15 nm with a narrow size-spectrum ($\approx$ 20 nm) whereas, the SMLM reconstructed image has a relatively large mean size of $\approx$40 nm with a wide size-spectrum ($>$100 nm). Thus restricting molecules with large sizes (corresponding to large LPs) to participate in the image reconstruction process has resulted in a 3-fold improvement in resolution when compared to traditional SMLM methods. It may be noted that the number of molecules with size $<$10 nm are significantly few indicating the inability of POSSIBLE microscopy to reconstruct images with mean size $<$10 nm pertaining to the present dataset. However, a better dataset with ultra-bright molecules is capable of resolving clusters with a resolution of single-molecule length-scales. Upon data collection, the position (centroid) and the localization precision of single molecules are determined. 2D Gaussian is used to fit the recorded single molecules for which the values range from 0 to 255 [4]. Traditional SMLM use both highly and poorly resolved single molecules, resulting in overlapping PSFs. This appears as a continuous saturated pixels but essentially indicate unresolved features as shown in Fig 3C. On the other hand, POSSIBLE technique employs only highly resolved single molecules and ignores poorly resolved molecules resulting in better resolvability of clusters.

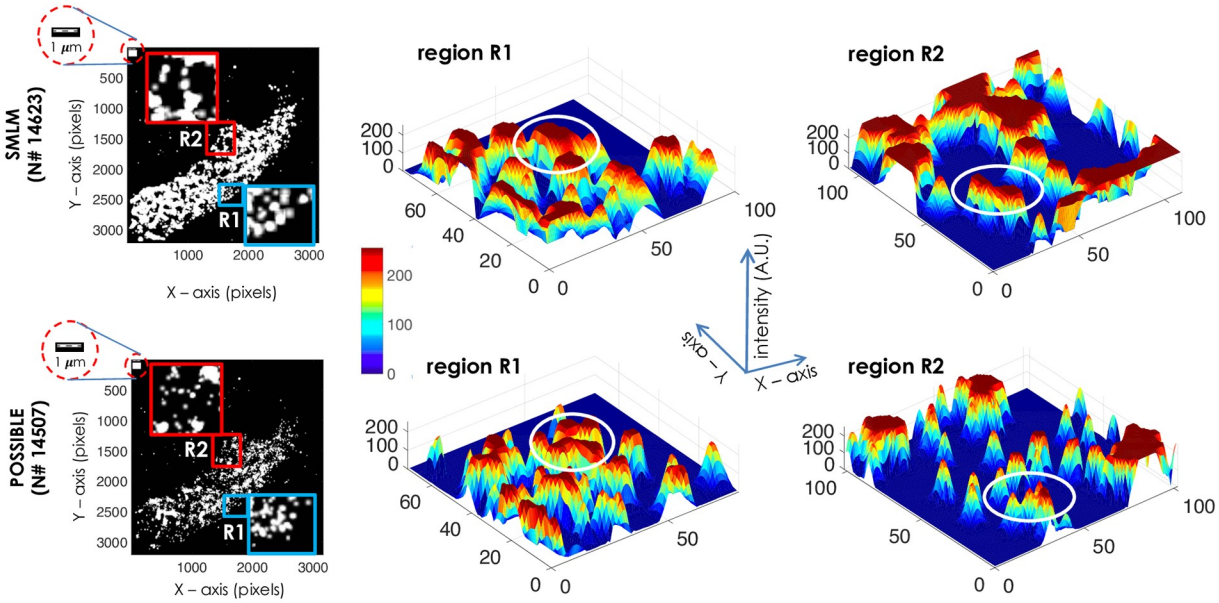

Fig 4. Cluster visualization. SMLM and POSSIBLE reconstructed images along with the zoomed version of two different clusters (marked by blue and red rectangles). 3D surface plot of two chosen clusters (marked by R1 and R2) are shown where the marked black ellipses indicate sub-clusters within large clusters. Visually, the resolving ability of POSSIBLE microscopy is quite apparent. Scale bar is 1 μm.

https://doi.org/10.1371/journal.pone.0242452.g004

So, POSSIBLE microscopy can in-principle provide unlimited resolution (spatial resolution of the actual size of single molecule), provided experimental detection of enough fortunate molecules is achieved.

The resolving capabilities of the POSSIBLE and SMLM microscopy can be visually demonstrated. We have chosen two different HA clusters (marked as R1 and R2 by the blue and red squares respectively) in the reconstructed map, and carried out 3D surface-plots (Fig 4). The zoomed version of the clusters along with 3D surface plots are also shown in Fig 4. SMLM reconstructed cluster show overlapping PSFs, whereas clusters reconstructed by POSSIBLE microscopy reveals relatively sparse PSFs. This is due to the involvement of small-sized PSFs (range, $5 - 25\ nm$ corresponding to $G(15\ nm, 10\ nm)$) of fortunate molecules in the cluster formation that gives resolution boost to POSSIBLE microscopy. On the other hand, SMLM builts the reconstruction map with PSFs having large size-spectrum ($10\ nm - 100\ nm$). The white circles show appearance of sub-clusters within large clusters as revealed by POSSIBLE microscopy which are otherwise poorly resolved by SMLM. Note that, regions with larger saturated values represent overlap of larger number of poorly resolved molecules (with large PSF) in close proximity. This suggests that POSSIBLE microscopy is better suited for resolving molecular clusters than standard SMLM.

C. HA cluster analysis

Clustering during influenza infection is critical to access its current state and progression rate. The reconstructed data (see, Fig 2) shows clustering of single molecules 24 Hrs post-transfection. Many factors contribute to the clustering of HA molecules and the consequent increase in cluster-size. In addition, the determination of number of HA molecules in a cluster is critical and has a strong influence on the rate of infection. These studies require optical microscopes that can resolve molecular clusters.

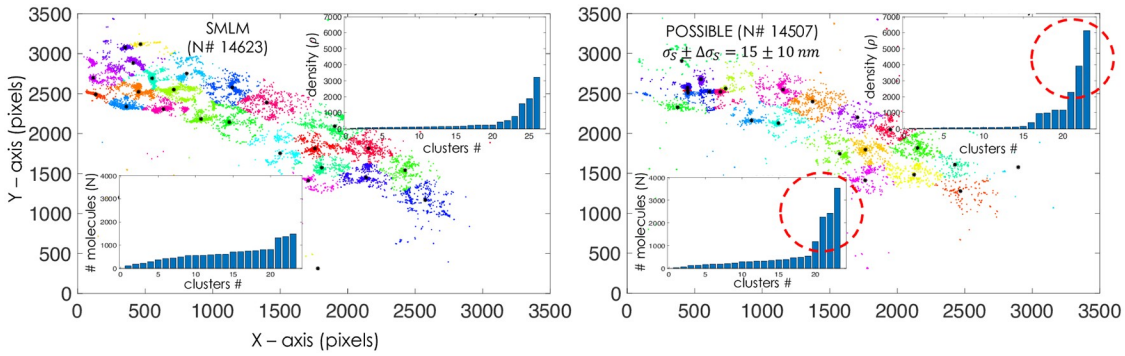

Fig 5. Cluster analysis using K-means clustering algorithm for SMLM and POSSIBLE microscopy (with filter, $G(\sigma_s, \Delta\sigma_s)$). Cluster density and HA number analysis are also shown in the inset. Other important parameters such as, cluster area, molecule packing and cluster-spread density are discussed in **Supplementary 2-4** of S1 File. The red circle indicates high-density and large molecule clusters for POSSIBLE reconstructed images ($G(\sigma_s, \Delta\sigma_s)$) that is missing for SMLM reconstructed images.

https://doi.org/10.1371/journal.pone.0242452.g005

Our study with NIH3T3 fibroblast cell lines using photoactivable HA molecules (Dendra2-HA) show high-resolution image of HA distribution. In order to elucidate the potential of POSSIBLE microscopy, we study cluster size, # HA molecules per cluster, cluster density, HA-HA proximity and its distribution. Raw data of single molecules is analyzed post-reconstruction followed by Matlab based rendering algorithms [12, 13, 28]. The clustering process begins by obtaining the location information of rendered single molecules (x and y positions) from the master data-matrix that contains other information such as, localization precision and the number of detected photons per molecule. The location information is fed to the developed clustering algorithm primarily based on k-means clustering (see, Matlab scripts). Fig 5 shows multiple clusters along with their centroids for POSSIBLE ($G(15\ nm, 10\ nm)$). The clusters are color-coded with their centroids marked by $'*'$. Since the clusters occur in all shapes, it is difficult to uniformly determine its size assuming isotropic spread of the cluster. So, we preferred to study cluster area rather than cluster size in the present work.

The insets in Fig 5 show K-means clustered data along with cluster-density analysis (the number of molecules ($\#N$) versus cluster number (Cluster #)) and the number-analysis (number of molecules per cluster). One can readily see that some clusters in SMLM reconstructed map looks elongated, however POSSIBLE reconstructed image show the presence of sub-clusters that are more compact and alike. There is a spike (indicated by red-dotted circle) in the number of HA molecules and cluster density which indicates compact and dense clustering post 24 Hrs of transfection. Moreover, there is a sharp decrease in large-sized clusters (of area $\approx 6\ \mu m^2$) in POSSIBLE reconstructed map ($\sigma_S \pm \Delta\sigma_S = 15 \pm 10\ nm$) as compared to SMLM reconstructed map (S2 Fig in **Supplementary 2** of S1 File). Analysis show the dominance of mid-size clusters (of area $1 - 4\ \mu m^2$) with the appearance of sizable large clusters (of area $\approx 6\ \mu m^2$) as shown in **Supplementary 2** of S1 File. This represents critical stage of clustering process post 24 Hrs since, the transfected cells were cultured for 24 Hrs followed by fixation. This observation is significant because large assembly of HA are known to occur much beyond 24 Hrs of infection.

A detailed comparison of SMLM and POSSIBLE microscopy for $(\sigma, \Delta\sigma) = (15nm, 10nm)$, $(30nm, 2nm)$, $(50nm, 2nm)$, respectively can be found in **Supplementary 1** of S1 File. K-means clustering suggests a total of 26 and 23 clusters, (including sparse ones) respectively for POSSIBLE and SMLM. The size of the clusters have ranged from $0.5 - 6\ \mu m^2$ (see, **Supplementary 2** of S1 File) and the number of HA molecules per cluster range from few hundred to few thousand (see, **Supplementary 3** of S1 File). Cluster-density analysis indicates the presence of few

highly-dense clusters (about 8%) and the rest 92% clusters are of low density (< 600 molecules). Other analysis corroborating the above observation is the cluster spread-density (total HA molecules per cluster spread-area) that shows a similar trend (see, **Supplementary 4** of S1 File). In addition to determine cluster-spread and proximity interactions, we ascertain that pairwise HA-HA distance (d) metric is a suitable metric as discussed in **Supplementary 5** of S1 File. The distance histogram (see, S5 Fig of S1 File) indicates that the spread is more confined and HA-HA interaction is high for POSSIBLE when compared to SMLM, thereby revealing the true nature of HA cluster formation post 24 Hrs of transfection. Overall, the studies suggest strong clustering, whereas dense clusters are better enunciated by POSSIBLE microscopy. The study also indicates the presence of medium-sized clusters (see, **Supplementary 4** of S1 File), and the existence of clusters with densely-packed HA molecules. We attribute this to the ability of POSSIBLE microscopy that employs relatively small-sized PSFs for the reconstruction of super-resolution map. The study shows the appearance of dense HA clusters post 24 Hrs of transfection. This is in consistence with the observation that dense packing of HA (influenza viral membrane protein Hemagglutinin) is essential for infectivity [27, 29, 30, 31].

III. Methods and protocols

A. POSSIBLE microscopy: Optical setup

POSSIBLE microscopy is built upon the standard localization microscopy (SMILE / fPALM) [4, 13]. The schematic diagram depicting the key components of the microscope and associated computational processes are shown in Fig 1. A laser light of wavelength, $\lambda_{acv} = 405\ nm$ (Oxxius, France) was used to randomly activate the molecules and a second laser of wavelength, $\lambda_{exc} = 561\ nm$ (Oxxius, France) was used for exciting the molecules. We used a high numerical aperture (NA) objective (Olympus 1.3NA, 100X) for both illuminating the sample and collecting the fluorescence photons from single molecules. The molecules (Dendra2HA) have an emission peak at 573 *nm*. A filter-cube containing dichroic filter and bandpass filter (from Shemrock, USA) was used to direct the light to specimen and filter-out fluorescence. An additional set of filters were employed in the detection path (Notch filters, 405 nm and 561 nm from Shemrock, USA) to block the back-reflected laser lights. Other optical components such as, mirrors, beam-splitters and opto-mechanical components were purchased from Thorlabs, Newton, NJ. The images were recorded using an Andor 897 iXon Ultra camera (Andor Technology, UK).

During experimentation, a large number of images (about 10000) were recorded and was followed by computational processing. The raw data was recorded by the EMCCD detector (Andor 897 iXon Ultra) and subjected to analysis for identifying single molecules (see, white boxes in Fig 1B). Subsequently, important parameters (such as, detected photons per molecule, centroid, molecule position, variance and others) were extracted from the analysis. A range for the size of molecules was preset to remove random noise (from the acquired images) and pixel-to-photon conversion was carried-out. The extracted data was then subjected to Gaussian filter (using Gaussian probability distribution function) to filter-out unfortunate molecules and retain the fortunate ones. The fortunate molecules are represented by black square boxes as shown in Fig 1B. The final step involves the reconstruction of single molecule image (termed as, POSSIBLE ultra-superresolution image) from the detected fortunate molecules.

All the experimental procedures were reviewed and approved by the Institutional Committee (IC), Indian Institute of Science. We declare that, all methods were carried out in accordance with relevant guidelines and regulations approved by Institutional Committee (IC) and Ethical Committee, Indian Institute of Science.

B. Gaussian filter and fortunate molecules

The key to multi-resolution POSSIBLE microscopy is the identification of fortunate molecules. A Gaussian probabilistic function is utilized to determine the size-spectrum of molecules needed to reconstruct the map. In general, molecules are defined by their centroid position and localization precision (say, σ) which determines their size [32]. Localization precision is used to determine the position uncertainty around the centroid of molecule that fixes its size. For convenience, we define three sets of molecules with mean LP (σ) and its variance $\Delta\sigma$. Accordingly, we choose to work with Gaussian distribution. Three Gaussian distributions in the (σ, $\Delta\sigma$)-space were chosen say, (σ_s, $\Delta\sigma_s$), (σ_m, $\Delta\sigma_m$) and (σ_l, $\Delta\sigma_l$) which represent highly-, moderately- and poorly- resolved molecules, respectively. This is as shown in Fig 2B (see, insertion). It may be noted that, mean and variance of the distribution, $G(\sigma, \Delta\sigma)$ need to be predefined and thereafter the process for finding the fortunate molecules needs to be initiated. The molecule that falls in a specific Gaussian distribution (say, $G(\sigma_s, \Delta\sigma_s)$ or $G(\sigma_m, \Delta\sigma_m)$ or $G(\sigma_l, \Delta\sigma_l)$) are designated as fortunate in the respective range (σ, $\Delta\sigma$). For example, if the application desires $\sigma = 15\ nm$ with a variance of say, $\Delta\sigma = 10\ nm$, the fortunate molecules are the ones that fall in the range ($[\sigma - \Delta\sigma, \sigma + \Delta\sigma] = [5\ nm, 25\ nm]$) and obey Gaussian distribution function $G(\sigma = 15\ nm, \Delta\sigma = 10\ nm)$. To generate multi-resolution map, more than one Gaussians need to be defined in the search space (σ, $\Delta\sigma$). Mathematically, we can define Gaussian as, $G(\sigma, \Delta\sigma) = A\ \exp\left[\frac{-(\sigma^2-\sigma_0^2)^2}{2\Delta\sigma}\right]$ where, σ_0 and $\Delta\sigma^2$ are respectively the mean and variance of the function. Here, the mean σ_0 represent average size of the fortunate molecules whereas, the variance $\Delta\sigma$ represent the size-spectrum of fortunate molecules. It may be noted that, the distribution is not symmetric. This is due to the fact that, POSSIBLE technique necessitates a lower and upper size bound to the original distribution for identifying fortunate molecules and does not influence the original distribution.

The Gaussian probability distribution function ensures that the molecule size (or equivalently LP) that is close to the average size σ_0 (average LP) are more likely to be considered as fortunate molecules than others that are far from it. Since the distribution theoretically extends from $-\infty$ to $+\infty$, we need to symmetrically fix a lower bound on the probability. We have chosen the corresponding probability as, $P_1 = 0.001$ which means molecules that have a probability $P > P_1$ are selected and termed as, fortunate molecules. These molecules contribute to the reconstructed image. For multiresolution POSSIBLE microscopy, we defined 3 distinct Gaussian distributions.

C. Biological sample prepration protocols

D. Cell culture

Standard protocol for culturing NIH3T3 fibroblast cells (source: Biological Sciences, Indian Institute of Science, Bangalore, India) were followed [13, 27]. The cells were thawn at low passage and grown overnight with complete growth media (80% DMEM + 10% calf bovine serum + 4.5 *ml* penicillin streptomycin). Subsequently, the medium was changed to reduce the toxicity caused by freezing medium (90% complete cell medium + 20% DMSO). A balanced protocol is followed to ensure that density of cells to be about $10^5/cm^2$ and a maximum confluency of about 80% is ensured for subsequent split followed by transfection with the Dendra2HA-plasmid-DNA.

E. Cell transfection and fixing

We have chosen to work with NIH3T3 cells for the proposed study [13, 33, 34]. NIH3T3 mouse fibroblast cells were transiently transfected with Dendra2-Hemagluttinin (HA) using Lipofectamine 3000 (Life Technologies, Invitrogen) as per the established protocol [27, 33, 35]. The constructs for photoactivable fluorescent protein (Dendra2) tagged with proteins of interest (Hemagglutinin), were plated in a 35 mm disc (with coverslips at the bottom) (Thermofisher Scientific). Cells were grown to the confluency of ≈ 80% and cleaned with phosphate-buffered saline (PBS). Before proceeding with labeling, cells were checked under transmission light microscope for normal morphology. Subsequently, the cells were fixed with 4% PFA. Post-fixing the cells were sealed with another coverslip using fluorosave solvent (Thermofisher Scientific) for long-time preservation and imaging. The cells were then imaged with high-resolution inverted fluorescence microscope equipped with a broad blue light source (of wavelength in the range, 470-490 nm) and appropriate filter-set is used to observe the green fluorescence (emission maximum, $\lambda = 507\ nm$) from the transfected cells. This confirms the expression of Dendra2-HA protein in the cell. These cells were subsequently selected and imaged with superresolution microscope (POSSIBLE and SMLM).

F. Superresolution imaging

Typically, 10,000 frames were recorded at 30 Hz and with an EM gain of 250. The activation (wavelength, $\lambda = 405\ nm$) and excitation (wavelength, $\lambda = 561\ nm$) laser powers used at the sample were 112 μW and 6.3 mW, respectively. A total of 173448 molecules were recorded with an average rate of ≈17.3 single molecules per frame (see, S1 Video). This was followed by particle-size filtering to remove false counting and photon-count filtering to get rid of random background and very weak emitters. Finally, the single molecules were filtered using Gaussian filter to obtain fortunate molecules. We observed that some of single molecule frames does not have fortunate molecules while other frames may have 1–3 fortunate molecules. On an average, approximately 1.45 fortunate molecules per frame were extracted from single molecule frames (see, S2 Video).

Post fixation to the coverslips, cells were imaged using the super-resolution microscope [12, 13]. The molecules thus recorded in several frames were analyzed and localized using developed protocols [28]. Major computational tasks involve spot-identification (that indicate emission from a single molecule), thresholding (to eliminate the background) and Gaussian-fit (for identifying single molecules). The analysis determines centroid and variance of the fitted Gaussian giving the location and localization precision of the single molecule. The size of single molecule was determined from its localization precision. Subsequently, single molecule ensembles were subjected to cluster analysis.

G. K-means clustering of HA molecules and cluster properties

The single molecule analysis of raw data determines a total of 173448 molecules for which the positions and localization precision were calculated. A size-based filtering is carried out to filter noisy pixels. This is based on the fact that, less than 3 × 3 pixels window on the camera chip may not represent single molecule and so the Gaussian-fit to determine its size is not appropriate, whereas larger than 9 × 9 pixel window may represent two or more close-by single molecules. This is followed by Gaussian filter to filter-out unfortunate molecules. The remaining fortunate molecules belonging to $G(\sigma_l, \Delta\sigma_l)$, $G(\sigma_m, \Delta\sigma_m)$ and $G(\sigma_s, \Delta\sigma_s)$ are 14042, 18562 and 14507, respectively. These molecules were used to reconstruct the respective super-resolved image. Post reconstruction, the clusters were determined by K-means method (inbuilt MATLAB scripts). We identified about 26 clusters for SMLM reconstructed images whereas, 23, 22 and 25 clusters were observed respectively for $G(15\ nm, 10\ nm)$, G(30 *nm*, 2 *nm*), G(50

nm, 2 *nm*) (see, **Supplementary 1** of S1 File). This formed the basis for cluster area analysis and the number of HA-molecules per cluster (see, **Supplementary 2 and 3** of S1 File).

Clustering involves the knowledge of position coordinate of single molecules that lie within the same cluster. We used K-means clustering which is an unsupervised learning method. However, it is iterative in nature that begins with an initial guess for the centroids (of the clusters) and the iterations continues until there is no change to the centroids. K-means use nearest-neighbour method (cityblock) that use sum of absolute differences (L1 distance) for clustering data-points and the centroid is median of points in the cluster. This enables, the determination of important clustering parameters related to influenza infection such as, the cluster area, cluster-density and molecules per cluster. Unlike other implementations, specific shape of the cluster is not assumed for deducing these parameters. This helps in a better estimation of important parameters related to clustering.

In addition, MATLAB K-means script allow determination of sum of point-to-centroid distances for each cluster. The average point-to-centroid distance physically indicates the effective area over which the cluster is spread. So, spread-density of a cluster is an important parameter for accessing the spread post 24 Hrs of transfection. The cluster-spread density study indicates 6-fold increase in spread-density for POSSIBLE microscopy as compared to traditional SMLM (see, **Supplementary 4** of S1 File).

IV. Discussion

POSSIBLE superresolution microscopy is a powerful and unique methodology for an in-principle **resolution of the order of actual single molecule size**. The key that holds the superior resolution is the number of photons emitted by the molecule. This has a direct bearing on the localization-precision ($\Delta_{lp} = \Delta_{psf}/\sqrt{N}$) of the molecule, where Δ_{psf} is the diffraction-limited PSF and N is the number of emitted photons. It is quite clear that to gain better resolution, the molecule need to be bright and should be capable of emitting a large number of photons. We call these extra-ordinary bright molecules as **fortunate molecules**. The brightness of a molecule is the product of quantum efficiency and extinction coefficient (that in turn depend upon transition dipole moment and local environment (solvent) that are free from oxygen species leading to photobleaching) [36]. Thus with the availability of large emitted photons, the position of molecules can be better localized. This ultimately results in small PSF for fortunate molecules. A large collection of fortunate molecules can then be used to reconstruct the map which becomes the basis to understand biological processes and determine underlying mechanisms with enhanced resolution.

The central idea is to identify fortunate molecules and built-up enough statistics to reconstruct **ultra-superresolved image**. Such a technique would be able to resolve molecular clusters. Fig 5 demonstrates this by resolving large aggregates / clusters showing molecular compactness, cluster density, cluster spread and HA-HA proximity. The ultra-superresolved molecular map generated by POSSIBLE microscopy enables detailed study of molecular clusters which are not possible by traditional localization microscopy (fPALM/PALM). Our study has revealed existence of sub-clusters within large clusters (see, Fig 4) and HA-HA interaction, thereby revealing the true nature of HA-assembly post 24 Hrs of transfection. K-means clustering (inbuilt MATLAB scripts) is exploited to determine the aggregation process and calculate cluster size (or equivalently cluster area), HA molecules per cluster and spread-density (see, **Supplementary 1-5** of S1 File). These parameters suggest that post 24 Hrs of transfection, clustering happens in phases with the formation of small sub-clusters (size 1–2 μm^2) before joining together to form large clusters (size $\approx$6 μm^2). This is important because small clusters relate to mild infection and drugs can be targeted to prevent large clustering (indication of strong

infection). A similar study demonstrates the effect of actin-disrupting drugs on the morphology of HA clusters in Dendra2-HA-transfected NIH3T3 cells [27].

Another important parameter is the number of HA molecules in clusters which is critical to virion maturation followed by its exit from the infected cell. Here, the traditional SMLM super-resolution microscopy is unable to predict the appearance of these densely-packed clusters, whereas POSSIBLE microscopy shows the presence of dense clusters. In addition, sub-clusters are found in elongated large HA clusters. We attribute this to the ability of POSSIBLE microscopy that can produce better-resolved molecular maps. These observed sub-clusters range from few tens to few hundred nanometers lying within elongated HA clusters. Earlier studies using fPALM has revealed the presence of elongated clusters [27].

However, proposed methodology has disadvantages too: (1) since large statistics is sought and detection of fortunate molecules is a rare event so the hunting-time is large, requiring large acquisition time, (2) currently, not many super bright probes are available that can be conjugated with the protein of interest, and (3) POSSIBLE technique is strictly limited to fixed samples. In addition, a meaningful ultra-superresolution map can only be constructed with the availability of sufficient fortunate molecules. These limitations and the difficulty associated with in-vivo study of biological specimens is a handicap for this promising technique. On the bright side, it should be possible to design super bright non-toxic photoactivable probes that can be easily conjugated with the protein-of-interest for studying biological processes [37, 38].

Overall, POSSIBLE microscopy gains spatially by sacrificing the temporal resolution and hence it is ideally suitable for fixed-cell imaging. Multiresolution capability of POSSIBLE microscopy suggests that simultaneously many super-resolution map can be reconstructed. As an example, Fig 2 shows 3 different resolution regimes: highly-resolved (15±10 *nm*), moderately-resolved (30±2 *nm*) and poorly-resolved (50±2 *nm*), respectively. Traditional localization microscopy closely resembles poorly-resolved POSSIBLE microscopy with a large average LP and broad LP-bandwidth. This is further clear from the fPALM images and localization map shown in Fig 3. In addition, proposed technique is readily adaptable and integrable with the existing localization techniques. We envision that POSSIBLE microscopy has the ability to stretch the resolution to sub-10 nm for functional biological imaging.

Supporting information

S1 Video.
(AVI)

S2 Video.
(AVI)

S1 File.
(PDF)

Acknowledgments

The author thanks Prof. Samuel T. Hess, Department of Physics, University of Maine, Orono, USA for fruitful discussion on fPALM superresolution microscopy and support.

Author Contributions

Conceptualization: Partha Pratim Mondal.

Data curation: Partha Pratim Mondal.

Formal analysis: Partha Pratim Mondal.

Funding acquisition: Partha Pratim Mondal.

Investigation: Partha Pratim Mondal.

Methodology: Partha Pratim Mondal.

Project administration: Partha Pratim Mondal.

Resources: Partha Pratim Mondal.

Software: Partha Pratim Mondal.

Supervision: Partha Pratim Mondal.

Validation: Partha Pratim Mondal.

Visualization: Partha Pratim Mondal.

Writing – original draft: Partha Pratim Mondal.

Writing – review & editing: Partha Pratim Mondal.

References

1. Abbe E., Beitrge zur Theorie des Mikroskops und der mikroskopischen Wahrnehmung, Arch. f.Mikr. Anat. 9, 413–420 (1873). https://doi.org/10.1007/BF02956173
2. Born M., and Wolf E. 1997. Principles of Optics: Electromagnetic Theory of Propagation, Interference and Diffraction of Light. Cambridge University Press, Cambridge, UK.
3. Hell S. W., Wichmann J., Breaking the diffraction resolution limit by stimulated emission: Stimulated-emission-depletion fluorescence microscopy". Optics Letters 19, 780–782 (1994). https://doi.org/10.1364/OL.19.000780
4. Hess S. T., Girirajan T. P. K., and Mason M. D., Ultra-high resolution imaging by fluorescence photoactivation localization microscopy. Biophys. J. 91, 4258–4272 (2006). https://doi.org/10.1529/biophysj.106.091116
5. Rust M. J., Bates M., and Zhuang X., Sub-diffraction-limit imaging by stochastic optical reconstruction microscopy (STORM), Nature Methods 3, 793 (2006). https://doi.org/10.1038/nmeth929 PMID: 16896339
6. Betzig E., Patterson G. H., Sougrat R., Lindwasser O. W., Olenych S., Bonifacino J. S., et al. Imaging intracellular fluorescent proteins at nanometer resolution, Science 313, 1642–1645 (2006). https://doi.org/10.1126/science.1127344
7. Gustafsson M. G., Nonlinear structured-illumination microscopy: Wide-field fluorescence imaging with theoretically unlimited resolution, Proc. Natl. Acad. Sci. U.S.A. 102, 13081 (2005). https://doi.org/10.1073/pnas.0406877102 PMID: 16141335
8. Fölling J., Bossi M., Bock H., Medda R., Wurm C. A., Hein B., et al. Fluorescence nanoscopy by ground-state depletion and single-molecule return, Nature Methods 5, 943 (2008). https://doi.org/10.1038/nmeth.1257
9. Dertinger T., Colyer R., Iyer G., Weiss S., and Enderlein J., Fast, background-free, 3D super-resolution optical fluctuation imaging (SOFI), Proc. Natl. Acad. Sci. USA 106, 22287 (2009). https://doi.org/10.1073/pnas.0907866106
10. Sharonov A. and Hochstrasser R. M., Wide-field subdiffraction imaging by accumulated binding of diffusing probes, Proc. Natl. Acad. Sci. USA 103, 18911–18916 (2006). https://doi.org/10.1073/pnas.0609643104
11. Giannone G., Hosy E., Levet F., Constals A., Schulze K., Sobolevsky A. I., et al. Dynamic superresolution imaging of endogenous proteins on living cells at ultra-high density, Biophys. J. 99, 1303–1310 (2010). https://doi.org/10.1016/j.bpj.2010.06.005
12. Mondal Partha P., Simultaneous multiplane imaging-based localization encoded (SMILE) microscopy for super-resolution volume imaging, Micros. Res. Tech. 80, 333 (2017). https://doi.org/10.1002/jemt.22828 PMID: 28106304

13. Mondal Partha P. and Hess Samuel T., Total internal reflection fluorescence based multiplane localization microscopy enables super-resolved volume imaging, App. Phys. Lett. 110, 211102 (2017). https://doi.org/10.1063/1.4983786

14. Gwosch K. C., Pape J. K., Balzarotti F., Hoess P., Ellenberg J., Ries J. et al. MINFLUX nanoscopy delivers 3D multicolor nanometer resolution in cells, Nature Methods 17, 217–224 (2020). PMID: 31932776

15. Zhang Y., Schroeder L. K., Lessard M. D., Kidd P., Chung J., Song Y., et al. Nanoscale subcellular architecture revealed by multicolor three-dimensional salvaged fluorescence imaging, Nature Methods 17, 225–231 (2020). https://doi.org/10.1038/s41592-019-0676-4

16. Karmen AbuZineh, Joudeh Luay I., Al Alwan Bader, Hamdan Samir M., Merzaban Jasmeen S. et al. Microfluidics-based super-resolution microscopy enables nanoscopic characterization of blood stem cell rolling, Science Advances 4, eaat5304 (2018). https://doi.org/10.1126/sciadv.aat5304

17. Mlodzianoski M. J., Future Considerations for Localizationbased Super-resolution Fluorescence Microscopy, iSci. Note., 1 5 (2016).

18. Thevathasan Jervis Vermal, Kahnwald Maurice, Cieśliński Konstanty, Hoess Philipp, Peneti Sudheer Kumar, Reitberger Manuel, et al. Nuclear pores as versatile reference standards for quantitative super-resolution microscopy, Nature Methods 16, 1045–1053 (2019). https://doi.org/10.1038/s41592-019-0574-9 PMID: 31562488

19. Habuchi Satoshi, Microfluidics-based Super-Resolution Imaging: A New Tool for Nanoscopic Charactertization of Cellular Interactions, iSci. Note., 4 1 (2019).

20. Ma Hongqiang, Xu Jianquan and Liu Yang, WindSTORM: Robust online image processing for high-throughput nanoscopy, Science Advances 5, eaaw0683 (2019). https://doi.org/10.1126/sciadv.aaw0683 PMID: 31032419

21. Turcotte Raphaël, Liang Yajie, Tanimoto Masashi, Zhang Qinrong, Li Ziwei, Koyama Minoru, et al. Dynamic super-resolution structured illumination imaging in the living brain, PNAS 116, 9586 (2019). https://doi.org/10.1073/pnas.1819965116 PMID: 31028150

22. Valles M. and Hess S. T., A cross beam excitation geometry for localization microscopy, iSci. Note., 2 1 (2017).

23. Wang Chenguang, Taki Masayasu, Sato Yoshikatsu, Tamura Yasushi, Yaginuma Hideyuki, Okada Yasushi, et al. A photostable fluorescent marker for the superresolution live imaging of the dynamic structure of the mitochondrial cristae PNAS 116, 15817 (2019). https://doi.org/10.1073/pnas.1905924116 PMID: 31337683

24. White J., Helenius A., and Gething M. J. Haemagglutinin of influenza virus expressed from a cloned gene promotes membrane fusion. Nature. 300, 658–659 (1982). https://doi.org/10.1038/300658a0

25. Chen B. J., Leser G. P., Morita E., Lamb R. A., Influenza virus hemagglutinin and neuraminidase, but not the matrix protein, are required for assembly and budding of plasmid-derived virus-like particles. J. Virol. 81, 7111–7123 (2007). https://doi.org/10.1128/JVI.00361-07

26. Hess S. T., Gould T. J., Gudheti M. V., Maas S. A., Mills K. D., Zimmerberg J., Dynamic clustered distribution of hemagglutinin resolved at 40 nm in living cell membranes discriminates between raft theories. Proc. Natl. Acad. Sci. USA. 104, 17370–17375 (2007). https://doi.org/10.1073/pnas.0708066104

27. Gudheti Manasa V., Curthoys Nikki M., Gould Travis J., Kim Dahan, Gunewardene Mudalige S., Gabor Kristin A., et al. Actin Mediates the Nanoscale Membrane Organization of the Clustered Membrane Protein Influenza Hemagglutinin, Biophys. Jl. 104, 2182–2192 (2013). https://doi.org/10.1016/j.bpj.2013.03.054

28. Mondal Partha P., Curthoys Nikki M. and Hess Samuel T., Clean localization super-resolution microscopy for 3D biological imaging, AIP Advances 6, 015017 (2016). https://doi.org/10.1063/1.4941075

29. Rein A., McClure M. R., Rice N. R., Luftig R. B., Schultz A. M., Myristylation site in Pr65gag is essential for virus particle formation by Moloney murine leukemia virus. Proc. Natl. Acad. Sci. 83, 7246–7250 (1986). https://doi.org/10.1073/pnas.83.19.7246

30. Göttlinger H.G., SodroskiJ.G., Haseltine W.A. Role of capsid precursor processing and myristoylation in morphogenesis and infectivity of human immunodeficiency virus type 1. Proc. Natl. Acad. Sci. 1989; 86:5781–5785. https://doi.org/10.1073/pnas.86.15.5781

31. Bryant M., Ratner L., Myristoylation-dependent replication and assembly of human immunodeficiency virus, Proc. Natl. Acad. Sci. 87, 523–527 (1990). https://doi.org/10.1073/pnas.87.2.523

32. Thompson R. E., Larson D. R., Webb W. W., Precise Nanometer Localization Analysis for Individual Fluorescent Probes, Biophys. Jl. 82, 2775–2783 (2002). https://doi.org/10.1016/S0006-3495(02)75618-X

33. Mlodzianoski M. J., Curthoys N. M., Gunewardene M. S., Carter S., Hess S. T., Super-Resolution Imaging of Molecular Emission Spectra and Single Molecule Spectral Fluctuations Plos One 11, e0147506 (2016). https://doi.org/10.1371/journal.pone.0147506

34. Parent M., Hess Samuel T., Quantification of mitochondrial membrane curvature by three-dimensional localization microscopy, ISci. Note. 4, 3 (2019). https://doi.org/10.22580/iSciNoteJ4.4.3

35. Ellens H., Bentz J., White J. M., Fusion of influenza hemagglutinin-expressing fibroblasts with glycophorin-bearing liposomes: role of hemagglutinin surface density. Biochemistry. 29, 9697–9707 (1990). https://doi.org/10.1021/bi00493a027

36. Song L. L., HenninkIan E.J., Young I T, Tanke H. J, Photobleaching Kinetics of Fluorescein in Quantitative Fluorescence Microscopy, Biophysical Journal 68(6):2588–600 (1995). https://doi.org/10.1016/S0006-3495(95)80442-X PMID: 7647262

37. Kwon Jiwoong, Park Jong-Seok, Kang Minsu, Choi Soobin, Park Jumi, Kim Gyeong Tae, et al. Bright ligand-activatable fluorescent protein for high-quality multicolor live-cell super-resolution microscopy, Nature Comm. 11, 273 (2020). https://doi.org/10.1038/s41467-019-14067-4 PMID: 31937765

38. Banaz Nehir, Mäkelä Jarno, and Uphoff Stephan, Choosing the right label for single-molecule tracking in live bacteria: side-by-side comparison of photoactivatable fluorescent protein and Halo tag dyes, J Phys D Appl Phys. 52, 064002 (2019). https://doi.org/10.1088/1361-6463/aaf255 PMID: 30799881